A new scenario applying traffic flow analogy to poleward expansion of auroras

Osuke Saka

Office Geophysik, Ogoori, Japan

Abstract

Transient westward electric fields from the magnetosphere generate equatorward plasma drifts of the order of kilometers per second in the auroral ionosphere. This flow channel extends in north-south directions and is produced in the initial pulse of Pi2 pulsations associated with the field line dipolarization. Drifts in the ionosphere of the order of kilometers per second that accumulated plasmas at the low latitude end of the flow channel are of such large degree that possible vertical transport effects (including precipitation) along the field lines may be ignored. We suggest that plasma compression in the ionosphere implemented the ionosphere active. The active ionosphere includes a nonlinear evolution of the compressed ionospheric plasmas, field-aligned currents to satisfy the quasi-neutrality of the ionosphere, and parallel potentials associated with the excitation of an ion acoustic wave. We will study how the active ionosphere created auroral expansion.

1. Introduction

"Auroras and solar corona observed at the solar eclipse are optical phenomena unique in space physics. With enough knowledge about the underlying physical processes, once auroras have been captured by a highly sensitive imager, they provide an unexpected wealth of information about plasma environment of the Earth" [Oguti, 2010]. Plasma drifts in the ionosphere observed by the balloon-measured electric fields [Kelley et al., 1971], by the Ba releases [Haerendel, 1972] and by radar observations [Nielsen and Greenwald, 1978] did not match the expanding trajectories of auroras.

These were observed in all-sky images as violent motion of auroras propagating poleward [Akasofu et al., 1966] and contact breakups initiated at the nearest approach to the hydrogen arc [Oguti, 1973]. To account for the difference in propagation directions, it was suggested that the primary sources of auroral particles are in the magnetospheric plasmas and they developed poleward in terms of propagation of rarefaction wave in the tail [Chao et al., 1971; Liu et al., 2012], tailward regression/braking of the fast earthward flows referred to as BBFs [Shiokawa et al., 1997; Haerendel, 2015], and onset instability of inner plasma sheet pressure [Nishimura et al., 2010]. It is suggested that substorm expansion was initiated and amplified at the substorm onset by the BBFs arriving at the inner boundary of plasma sheet from the tail [Kepko et al., 2004; Angelopoulos et al., 2008; Machida et al., 2009].

We will show that the electric fields in the dipolarization front (DF) [Runov et al., 2011] amplified by the projections into the auroral ionosphere yield the compressibility in auroral ionosphere. The compressibility initiates the active ionosphere and leads to an alternative scenario of the poleward expansion of auroras. In this paper, field line reconfiguration at dipolarization onset and associated auroral breakups will be summarized in section 2. In section 3, we will show that the auroral ionosphere becomes compressive transiently during dipolarization. Section 4 will discuss generation of an ion acoustic wave for creating parallel potentials in the topside ionosphere. Poleward expansion of discrete auroras will be discussed in section 5 in terms of a nonlinear evolution of the accumulated plasmas in the ionosphere. In the final section (section 6), we summarize our results and apply "the active ionosphere" to the nonconjugate auroras.

2. Auroras and field line reconfiguration associated with Pi2

In the waveform of Pi2 pulsations, poleward expansion of auroras arising out of the onset arc was observed in the initial pulse of Pi2 pulsations [Saka et al., 2012]. Statistical study of field line inclinations at geosynchronous orbit for the intervals from 120-min prior to the Pi2 onset (T-120) to 60-min after the onset (T+60) is presented in Figure 1 (reproduced from [Saka et al., 2010]). The inclination is measured positive northward from the D-V plane of the HVD coordinates. H is positive

northward parallel to dipole axis, V is radial outward, and D is dipole east. It shows that field line inclination at geosynchronous orbit (Goes5/6 at 285°/252° in geographic coordinates) decreased continuously in the growth phase and attained minimum inclination angles, 33.6°/49.4°, 2-min prior to the initial peak of Pi2 amplitudes. These inclination angles are smaller than 57.5°/63.8° estimated by the IGRF (International Geomagnetic Reference Field) model but rather fit the T89 model [Tsyganenko, 1989] of Kp=4 (34.2°/45.0°). These field lines at the geosynchronous altitudes can be mapped to auroral ionosphere at 63.4°N/62.7°N in geomagnetic coordinates by T89 for Kp=4. From these estimations, we postulate that BBFs reaching geosynchronous orbit activated preonset auroras at 63.4°N/62.7°N by the transmission of electric fields from the dipolarization front (DF) embedded in the initial pulse of the BBFs [Runov et al., 2011]. These transient electric fields were observed by the geosynchronous satellites as the convection enhancement of the plasma sheet electrons due to local breakdown of the last open trajectories of plasma sheet electrons [Thomsen et al., 2002]. The convection enhancement occurred in all-sky image coincident with the onset of bead-like rippling that leads to the breakups at the equatorward latitudes [Saka et al., 2014]. In the following Pi2 pulses, an auroral surge was observed in all-sky images between 66°N to 74°N in geomagnetic latitudes referred to as Poleward Boundary Aurora Surge (PBAS) [Saka et al., 2012]. They propagated eastward or westward at the poleward boundary of the auroral zone and were interpreted as an auroral manifestation of flow bifurcation of BBFs. In this onset scenario, the field line dipolarization finished in the initial pulse of the Pi2 pulsations, increasing field line inclination in a step-like manner for Goes5, and generating transient pulses for Goes6. The convection surge occurred once in the initial pulse of BBFs (DF) but is not repeated in the following pulses in the BBF train. This correlation suggests that auroral breakup may not repeat in the Pi2 wave packet but occurred at its initial pulse.

3. Horizontal plasma flows in the ionosphere

We assume that westward electric fields in the DFs that reached the vicinity of geosynchronous altitudes were transmitted along the field lines to the auroral ionosphere by the guided poloidal mode

[Radoski, 1967]. The electric fields in DFs would be amplified during the projection into the ionosphere over 100 mV/m and created an equatorward flow through $E \times B$ drift of the order of kilometers per second in the auroral ionosphere. Electric fields of the order of 100 mV/m generate these high velocity flows in the ionosphere. The flows would be confined in a channel expanding north-south in the midnight sector. The low-latitude end of the flow channel was at the latitudes of the onset arc. The high-latitude end may not expand beyond the poleward boundary of auroral zone. Longitudinal width of the flow channel may form a streamer [e.g., Nishimura et al, 2010] and develops after the breakups in about 1 to 2 hours of local time (~1000 km along 65 $^{\circ}$N) corresponding to horizontal scale size of plasma flow vortices associated with Pi2 [Saka et al., 2014].

In the flow channel, drift across the magnetic fields for the *j-th* species ($\mathbf{U}_{j\perp}$) can be written in the F region as [Kelley, 1989],

$$\mathbf{U}_{j\perp} = \frac{1}{B}[\mathbf{E} - \frac{k_B T_j}{q_j}\frac{\nabla n}{n}] \times \hat{\mathbf{B}} . \qquad (1)$$

Here, $\mathbf{E}$ denote westward electric fields in the flow channel and $\hat{\mathbf{B}}$ denotes a unit vector of the magnetic fields B , downward in the auroral ionosphere. Symbols k_B, T_j, q_j, and n are the Boltzmann constant, temperature of the *j-th* species, charge of the *j-th* species, and density of electrons (ions), respectively. The electric field of the order of 100 mV/m exceeded the diffusion (second term) by three orders of magnitudes in low temperature ionosphere. The $E \times B$ drift predominated in the F region and diffusion term may be ignored. In the E region, drift trajectories may be written [Kelley, 1989] for electrons by,

$$\mathbf{U}_{e\perp} = \frac{1}{B}[\mathbf{E} \times \hat{\mathbf{B}}] \qquad (2)$$

and for ions by,

$$\mathbf{U}_{i\perp} = b_i[\mathbf{E} + \kappa_i \mathbf{E} \times \hat{\mathbf{B}}] . \qquad (3)$$

Here, b_i is mobility of ions defined as $\Omega_i / (B\nu_{in})$, κ_i is defined as Ω_i / ν_{in} . Symbols Ω_i and ν_{in} are ion gyrofrequency and ion-neutral collision frequency, respectively. $\hat{\mathbf{B}}$ denotes a unit vector

of the magnetic fields B. To derive equations (2) and (3), pressure gradient term (diffusion) was again ignored. In the E region ($\kappa_i = 0.1$), although the first term of (3) exceeds the second term by one order of magnitudes, plasma accumulation in equatorward latitudes by the imposed westward electric fields was produced by equation (2) for electrons and the second term in (3) for ions. However, electron accumulation in lower latitudes increased southward electric fields and simultaneously ion drifts in the first term of (3). If the southward electric fields grew to exceed the westward electric fields by an order of magnitudes, ion drifts in the first term of (3) and electron drifts in (2) balanced to satisfy the quasi-neutrality. This is equivalent to the generation of the Pedersen currents in the ionosphere. Thus, electrostatic potential is generated in the E region, positive in poleward and negative in equatorward. The Pedersen currents would have closed to the field-aligned current (FAC), upward from the negative potential region and downward into the positive potential region to sustain the steady state electrostatic potential produced in the ionosphere. Plasma drifts in the ionosphere, both in E and F regions, create a cavity in the high-latitude end of the flow channel and accumulate density at the low-latitude end of the flow channel. We will focus on the density accumulation in the flow channel and discuss vertical transport of these accumulated materials. The development of the cavity in the flow channel may be the subject of another paper.

4. Vertical plasma flows in the ionosphere

A transient compression of the ionospheric plasmas at the low-latitude edge of flow channel would excite the ion acoustic wave in the ionosphere travelling along the field lines upward and downward directions from the density peak of the F region. Figure 2 shows altitude distribution of the pre-onset density profile of electrons (black) and density profile caused by the accumulation in red. The accumulation doubled the electron density profile from 90 km to 1000 km in altitudes. Electron density profile in black was plotted using sunspot maximum condition in nightside given in Prince and Bostic (1964). The travelling ion acoustic waves, upward and downward, are denoted by vertical arrows. Ion acoustic wave propagating downward may be eventually absorbed in the neutrals, while the upward wave may propagate along the field lines further upward. We will focus only on the upward

travelling ion acoustic wave. The ion acoustic wave produced the parallel electric fields in accordance with the Boltzmann relation [Chen, 1974],

$$E_{//} = -\frac{k_B T_e}{q}\frac{\nabla_{//} n_e}{n_e}. \qquad (4)$$

Here, k_B is Boltzmann constant, q is electron charge, T_e is electron temperature, and n_e is electron density ($n_e = n_i$). Equation (4) gives electric field strengths of the order of $0.4\mu V/m$ and $2.0\mu V/m$ for $T_e = 1000K$ and $T_e = 5000K$, respectively, when the e-folding distance of density dropout along the filed lines was 200 km. For ions, steady-state motions exist in the ionosphere in the altitudes where ion-neutral collision frequencies exceed ion acoustic wave frequencies. In that case, parallel motions can be written as [Kelley, 1989],

$$V_{i//} = b_i E_{//} - D_i \frac{\nabla_{//} n}{n} - \frac{g}{\nu_{in}}. \qquad (5)$$

Here, b_i and D_i denote mobility and diffusion coefficient of ions defined by $\frac{q_i}{M_i \nu_{in}}$ and $\frac{k_B T_i}{M_i \nu_{in}}$, respectively. Symbols, M_i, q_i, ν_{in}, and g are ion mass, electric charge of ions, ion-neutral collision frequency, and gravity, respectively. Ion-neutral collision frequencies from 400 km to 1000 km in altitudes were plotted in Figure 3 using nighttime sunspot maximum condition in Prince and Bostick (1964). Frequencies of ion acoustic wave were calculated by substituting wavelength of ion acoustic wave into the dispersion relation. The wavelength was assumed to be identical to initial accumulation distance along the field lines. We chose two cases of 1000 km and 4000 km. Phase velocity of the ion acoustic wave of the order of 1600 m/s for the electron temperatures of 5000K yields the wave frequencies of $1.6\times10^{-3}s^{-1}$ for the wavelength of 1000 km and $4.0\times10^{-4}s^{-1}$ for 4000 km. These frequencies were overlaid in Figure 3. Steady-state ion motions can be adopted up to 800 km, for a wavelength over 1000 km.

Altitude profile of steady-state ion flows were evaluated substituting 1000K for ion temperatures and the same e-folding distance in equation (4). Ions are oxygen and parallel electric fields are given

by the equation (4). A snapshot of the velocity profile in altitudes from 400 km to 800 km is shown in Figure 4 for the two cases of electron temperatures, 5000K for black dots and 1000K for red dots. For the low temperature case (1000k), there occurred no ion upflow because the parallel electric fields could not overcome gravity. We suggest that electron temperatures over 2700K would be needed to excite ion upflow. When electron temperature was set to 5000K, ion velocity 15 m/s at 400 km in altitudes increased rapidly to 1369 m/s at 800 km. The altitude profile of the flow velocity in Figure 4 matched Type 2 ion outflow observed by EISCAT radar [Wahlund et al., 1992]. We conclude that the ion upflow in topside ionosphere was caused primarily by the parallel electric fields excited by the upward travelling ion acoustic wave. Below 600 km in altitudes, upflow velocity was one-to-two orders of magnitudes smaller than the equatorward drift in the flow channel. Upflow velocity became comparable to the horizontal drift over 800 km in altitudes and exceeded the phase velocity of ion acoustic wave. Parallel velocity that prevailed the ion acoustic phase velocity may excite a shock at the topside ionosphere. A part of them developed to ion acoustic double layers [Sato and Okuda, 1980; Hasegawa and Sato, 1982; Hudson et al., 1983; Ergun et al., 2002] and were observed at the altitudes of 6000 – 8000 km [Mozer et al., 1976; Temerin et al., 1982]. Those ion acoustic double layers would have produced parallel potential structures referred to as inverted-V type electric fields.

5. Nonlinear evolution of the horizontal flows

Accumulation of electrons and ions occurred at the equatorward end of the flow channel. We can estimate a rate of accumulation by the following relation,

$$\frac{\Delta n}{\Delta t} = -n_0 \frac{\Delta U}{\Delta x} . \qquad (6)$$

Here n is plasma density, U denotes drift velocity in the flow channel in x. Substituting $\Delta U = 10^3 ms^{-1}$ and $\Delta x = 10^4 m$, we have $\frac{\Delta n}{\Delta t} = 10^{10} m^{-3} s^{-1}$ for the background density $n_0 = 10^{11} m^{-3}$. This gives density pileup of the order of $\frac{\Delta n}{n_0} = 100\%$ in ten seconds. If the

equatorward drift in the flow channel is an order of 10^3 m/s (E=100 mV/m in auroral ionosphere) and electron production by the precipitation do not exceed the accumulation rate which was 100% of the background density in ten seconds, both outflows and precipitation may not bring significant changes to the flux carried by $E \times B$ drift in the flow channel. We then approximate one dimensional (along the drift path in *x*) conservation equation in the flow channel.

$$\frac{\partial n}{\partial t} + \frac{\partial}{\partial x}(nU) = 0 \qquad (7)$$

A question arises regarding maximum accumulation of plasmas at the equatorward end of the flow channel because accumulation is limited. One possible mechanism to suppress accumulation may be associated with the ionospheric screening that decreased the amplitudes of penetrated (total) westward electric fields by the increasing ionospheric conductivities. In a two-dimensional ionosphere with uniform height-integrated conductivity, total electric fields *E* given by a sum of the incident (E_i) and reflected westward electric fields may be written as $E = \left(2\Sigma_A / \left(\Sigma_A + \Sigma_P\right)\right) E_i$, where Σ_A and Σ_P are Alfven conductance defined by $1/\mu_0 V_A$ and height-integrated Pedersen conductance in the ionosphere, respectively [Kan et al., 1982]. Symbols μ_0 and V_A denote magnetic permeability in vacuum and Alfven velocity, respectively. Amplitude ratio of total electric fields to incident electric fields is a function of conductance ratio of Pedersen and Alfven; $E/E_i = 2$ for a low conductivity of the ionosphere satisfying $\Sigma_P/\Sigma_A << 1$, and $E/E_i = 0$ for a high conductivity of the ionosphere satisfying $\Sigma_P/\Sigma_A >> 1$. Noting that Σ_P is proportional to the plasma density in the ionosphere, the total electric fields monotonically decreased with increasing plasma densities caused by accumulation itself and by the precipitations associated with the auroral activity. Another explanation may be suggested in the polarization electric fields (eastward) produced by the accumulation itself. These electric fields grew quickly with density accumulation and decreased the incident electric fields (westward) by the superposition. In addition to the above scenarios, we surmise that excess accumulation of the ionospheric plasmas may be suppressed through the term, $(\mathbf{U} \cdot \nabla)\mathbf{U}$, in the equation of motion. From the ionospheric screening process discussed above, we tentatively assume

that flow velocity U is a function of the density n. Then the conservation equation (7) may be written as,

$$\frac{\partial n}{\partial t}+\frac{\partial}{\partial x}Q(n)=0\,. \qquad (8)$$

Here, $Q(n)$ is a mass flux defined by $Q(n)=nU(n)$. This relation can be reduced to nonlinear wave equation,

$$\frac{\partial n}{\partial t}+c(n)\frac{\partial n}{\partial x}=0\,. \qquad (9)$$

Here $c(n)$ is a wave propagation velocity defined by $c(n)=U(n)+nU'(n)$, $U(n)$ is a drift velocity in the flow channel, and $U'(n)$ denotes braking/acceleration of the drift velocity by increasing and decreasing density. The equation (9) is often referred to as propagation of "kinematic waves" to describe traffic flow [Lighthill and Whitham, 1955]. In the following, we use dimensionless units normalized by U_{m}, and n_{m}. Here, U_{m} and n_{m} denote maximum drift velocity at n=0 and maximum density for complete stops of the drift, respectively. Assuming a constant braking in the flow channel, we define U by a linear function of density n as $U(n)$=1-n. Noting that $Q'(n)=c(n)$, this relation is reduced to the equation, $Q(n)=n(1-n)$, identical to the case for the traffic flow [Whitham, 1999]. Both the U and Q are plotted in Figure 5A as a function of n. A nonlinear evolution of the density waves is presented in Figure 5B by the characteristic curves. In the case of vehicles in traffic, the initial flows started from n=0 and stopped at n=1.0 by the tailback of cars. For the case of the ionosphere, the ionospheric density started from a finite density, n=0.3 in Figure 5B, and increased to n=1.0 to terminate the flow by the full screening. The nonlinear evolution of the density profile in time is shown in Figure 5B in colors from black ($T=T_1$), red ($T=T_2$), green ($T=T_3$), blue ($T=T_4$), and to purple ($T=T_5$). After $T=T_5$, the waves propagate upstream (poleward) as a shock. The shock velocity, V, is given as [Whitham, 1999],

$$V=\frac{Q(n_2)-Q(n_1)}{n_2-n_1}\,. \qquad (10)$$

Here, subscript 1 is for the values ahead shock and subscript 2 is for the values behind. Noting that

$Q(n_2)=0$ and substituting $Q(n_1)=n_1(n_2-n_1)$, the equation (10) can be reduced to $V=-n_1$ in dimensionless unit. The propagation velocity of the shock is related to the densities ahead. For the case of n=0.3 in Figure 5B, shock velocity can be estimated to be -0.3U_m. Here, U_m denotes maximum drift velocity in the ionosphere where ionospheric screening effects vanished by the condition, $\Sigma_P/\Sigma_A << 1$. The shock velocity may be of the order of kilometer per second, comparable but opposite to the equatorward drift in the flow channel.

6. Summary and Discussion

We proposed that the localized electric field drift introduced compressibility in the auroral ionosphere, which in turn generated field-aligned currents in the ionosphere for the quasi-neutrality, ion acoustic wave for parallel acceleration, and auroral expansions by nonlinear evolution of the ionospheric compression. We called the compressive ionosphere an active ionosphere.

We apply this active ionosphere to describe the asymmetry of discrete auroras in sunlit and dark hemispheres in the nightside sector (nonconjugate auroras). We suggest that asymmetry of the Pedersen conductance in sunlit and in dark ionosphere leads to the nonconjugate auroras. Weak electric fields in the sunlit auroral ionosphere would have caused a weak compressibility from which ion acoustic wave may not be excited or excited with only weak parallel potentials. This condition may reduce the occurrence probability of the discrete auroras and average energy of precipitating electrons in the sunlit hemisphere as exemplified in [Newell et al., 1996; Liou et al., 2001]. Weaker electric fields in the sunlit ionosphere may also require a longer interval to accumulate enough plasmas to excite ion acoustic wave. Such an instance is described in [Sato et al., 1998] where auroral breakups in sunlit ionosphere are delayed those in the dark hemisphere.

Finally, we note that poleward expansion as described here is an auroral event occurring in the initial pulse of Pi2 pulsations. In the succeeding pulses in the Pi2 wave trains, auroras are composed of poleward surge propagating at the poleward boundary of auroral zone (PBAS) [Saka et al., 2012]. We suppose that PBASs may be directly correlated to the reconnection processes inherent in the plasma sheet. This topic will be explored in another paper.

Acknowledgements

The author would like to express his sincere thanks to all the members of Global Aurora Dynamics Campaign (GADC) [Oguti et al., 1988]. We also gratefully acknowledge STEP Polar Network (http://step-p.dyndns.org/~khay/). Geomagnetic coordinates and footprints of the satellites are available at the Data Center for Aurora in NIPR (http://polaris.nipr.ac.jp/~aurora)

References

Akasofu, S.-I., Kimball, D.S., and Meng, C.-I.: Dynamics of the aurora-VII, Equatorward motions and the multiplicity of auroral arcs, J.Atmos.Terr.Phys., 28, 627-635, 1966.

Angelopoulos, V., et al.: Tail reconnection triggering substorm onset, Science, 321, 931, 2008.

Chao, J.K., Kan, J.R., Lui, A.T.Y., and Akasofu, S.-I.: A model for thinning of the plasma sheet, Planet.Space Sci., 25, 703-710, 1977.

Chen, F.F.: Introduction to plasma physics, Plenum Press, New York, 1974.

Ergun, R.E., et al.: Parallel electric fields in the upward current region of the aurora: Numerical solutions, Physics of Plasmas, 9, 3695-3704, 2002.

Haerendel, G.: Plasma drifts in the auroral ionosphere derived from Barium release, in Earth magnetospheric processes, B.M. McComac (ed), D.Reidel Publishing Company, 246-257, 1972.

Haerendel, G.: Substorm onset: Current sheet avalanche and stop layer, J.Geophys.Res., 120, doi10.1002/2014JA020571, 2015.

Hasegawa, A., and Sato, T.: Existence of a negative potential solitary-wave structure and formation of a double layer, Phys.Fluids, 25, 632-635, 1982.

Hudson, M.K., Lotko, W., Roth, I., and Witt, E.: Solitary waves and double layers on auroral field lines, J.Geophys.res., 88, 916-926, 1983.

Kan, J.R., Longenecker, D.U., and Olson, J.V.: A transient response of Pi2 pulsations, J.Geophys.Res., 87, 7483-7488, 1982.

Kelley, M.C., Starr, J.A., and Mozer, F.S.: Relationship between magnetospheric electric fields and the motion of auroral forms, J.Geophys.Res., 76, 5256-5277, 1971.

Kelley, M.C.: The earth's ionosphere: plasma physics and electrodynamics, Academic Press, Inc., 1989.

Kepko, L., Kivelson, M.G., McPherron, R.L., and Spence, H.E.: Relative timing of substorm onset phenomena, J.Geophys.Res., 109, doi:10.1029/2003JA010285, 2004.

Lighthill, M.J., and Whitham, G.B.: On kinematic waves. II. A theory of traffic flow on long crowded roads, Proc. R. Soc. Lond. A, 229, 317-345, 1955.

Liou, K., Newell, P.T., and Meng, C.-I.: Seasonal effects on auroral particle acceleration and precipitation, J.Geophys.Res., 106,5531-5542, 2001.

Liu, W.W., Liang, J., Donovan, E.F., and Spanswick, E.: If substorm onset triggers tail reconnection, what triggers substorm onset, J.Geophys.Res., 117, doi:10.1029/2012JA018161, 2012.

Machida, S., et al.: Statistical visualization of the arth's magnetotail based on Geotail data and the implied substorm model, AnnGeophys., 27, 1035-1046, 2009.

Mozer, F.S., Carlson, C.W., Hudson, M.K., Torbert, R.B., Parady, B., Yatteau, J., and Kelley, M.C.: Observations of paired electrostatic shocks in the polar magnetosphere, Phys.Rew.Lett., 38, 292-295, 1977.

Newell, P.T., Meng, C.I., and Lyons, K.M.: Suppression of discrete aurorae by sunlight, Nature, 381, 766-767, 1996.

Nielsen, E., and Greenwald, R.A.: Variations in ionospheric currents and electric fields in association with absorption spikes during substorm expansion phase, J.Geophys.Res., 83, 5645-5654, 1978.

Nishimura, Y., et al., Preonset time sequence of auroral substorms: Coordinated observations by all-sky imagers, satellites, and radars, J.Geophys.res., 115, doi:10.1029/2010JA015832, 2010.

Oguti, T.: Hydrogen emission and electron aurora at the onset of the auroral breakup, J.Geophys.Res., 78, 7543-7547, 1973.

Oguti, T., Kitamura, T., and Watanabe, T.: Global aurora dynamics campaign, 1985-1986, J.Geomag.Geoelectr, 40, 485-504, 1988.

Oguti, T.: Introduction to auroral physics (in Japanese), Laboratory for Solar-Terrestrial Environment, Nagoya University, 2010.

Prince, Jr., C.E., and Bostick, Jr., F.X.: Ionospheric transmission of transversely propagated plane waves at micropulsation frequencies and theoretical power spectrums, 69, 3213-334, 1964.

Radoski, H.R.: Highly asymmetric MHD resonances: The guided poloidal mode, J.Geophys.Res., 72, 4026-4027, 1967.

Runov, A., Angelopoulos, V., Zhou, X.-Z., Zhang, X.-J., Li, S., Plaschke, F., and Bonnell, J.: A THEMIS multicase study of dipolarization fronts in the magnetotail plasma sheet, J.Geophys.Res., 116, A05216, doi:10.1029/2010JA016316, 2011.

Saka, O. Hayashi, K, and Thomsen, M.: First 10 min intervals of Pi2 onset at geosynchronous altitudes during the expansion of energetic ion regions in the nighttime sector, J.Atmos.Solar Terr.Phys., 72, 1100-1109, 2010.

Saka, O., Hayashi, K., and Koga, D.: Periodic aurora surge propagating eastward/westward at poleward boundary of aurora zone during the first 10 min intervals of Pi2 onset, J.Atmos.Sol. Terr.Phys., 80, 285-295, doi:10.1016/j.jastp.2012.02.010, 2012.

Saka, O., Hayashi, K., and Thomsen, M.: Pre-onset auroral signatures and subsequent development of substorm auroras: a development of ionospheric loop currents at the onset latitudes, Ann. Geophys., 32, 1011-1023, 2014.

Sato, T., and Okuda, H.: Ion-acoustic double layers, Phys.Rev.Lett., 44, 740-743, 1980.

Sato, N., Nagaoka, T., Hashimoto, K., and Saemundsson, T.: Conjugacy of isolated auroral arcs and nonconjugate auroral breakups, J.Geophys.res., 103, 11641-11652, 1998.

Shiokawa, K., Baumjohann, W., and Haerendel, G.: Braking of high-speed flows in the near-Earth tail, Geophys.Res.Lett, 24, 1179-1182, 1997.

Temerin, M., Cerny, K., Lotko, W., and Mozer, F.S.: Observations of double layere and solitary waves in the auroral plasma, Phys.Rew.Lett., 48, 1176-1179, 1982.

Thomsen, M.F., Korth, H., and Elphic, R.C.: Upper cutoff energy of the electron plasma sheet as a measure of magnetospheric convection strength, J.Geophys.Res., 107, doi:10.1029/2001JA000148, 2002.

Tsyganenko, N.A.: A magnetospheric magnetic field model with a warped tail current sheet. Planet. Space Sci., 37, 5-20, 1989.

Whalund, J.-E., and Opgenoorth, H.J.: EISCAT observations of strong ion outflows from the F-region ionosphere during auroral activity: preliminary results, Geophys.Res.Lett., 16, 727-730, 1989.

Wahlund, J.-E., Opgenoorth, H.J., Haggstrom, I., Winser, K.J., and Jones, G.O.: EISCAT observations of topside ionospheric outflows during auroral activity: revisited, J.Geophys.Res., 97, 3019-3017, 1992.

Whitham, G.B.: Linear and nonlinear waves, A Wiley-Interscience Publication, JOHN WILEY & SONS, INC., 1999.

Figure Captions

Fig. 1: Inclination angles in degrees measured positive northward from the V-D plane from 120 min prior to the Pi2 onset (T-120) and to 60 min after the Pi2 onset (T+60) reproduced from Saka et al. (2010). Magnetometer data of Goes 5/6 were represented in HVD coordinates, H is positive northward parallel to dipole axis, V is radial outward, and D is dipole east. Epoch superposition of 30 Pi2 events and mean angles calculated from them are plotted in top and in lower panels, respectively. Mean inclination angle at 2-min before the initial peak of Pi2 amplitudes (T=0) was 33.6° for G5 and 49.4° for G6 in dipole coordinate. Dipolarization was step-like at 10.3°N (Goes5), while at 7.9°N (Goes6) it was composed of transient pulses.

Fig. 2: Vertical profiles from 90 km to 1000 km in altitudes of electron number density in two

conditions, pre-onset in black and after accumulation in red. Nighttime sunspot maximum condition given in Prince and Bostic (1964) was used to plot pre-onset condition. Vertical arrows directing upward and downward denote travelling ion acoustic waves propagating along the field lines from the density peak of F layer.

Fig. 3: Ion-neutral collision frequency (ν_{in}) in altitudes from 400 km to 1000 km calculated using nighttime sunspot maximum condition in Prince and Bostick (1964). Wave frequencies of ion acoustic wave are overlaid for two wavelength, 1000 km and 4000 km along field lines (see text).

Fig. 4: Steady-state parallel velocity in altitudes for ions (oxygen) produced by parallel electric fields $0.4\mu V/m$ (T_e=1000K) in red dots and $2.0\mu V/m$ (T_e=5000K) in black dots. Vertical flows in altitudes from 400 km to 800 km are shown. Flow velocity is positive upward and negative downward.

Fig. 5: (A) Normalized flux(Q)-density(n) curve (thin curve) and velocity(U)-density(n) line (thick line) in flow channel. Vertical scale of *U-n* line is shown to the right, scale of *Q-n* curve is to the left. Dotted line at n=0.5 indicates the critical density where *c(n)* vanishes; waves are stationary relative to the ground. Waves propagate forward/backward at a density below/above the critical density. (B) Nonlinear evolution of the density accumulation. Density increased in a step like manner from T_1 to T_5.

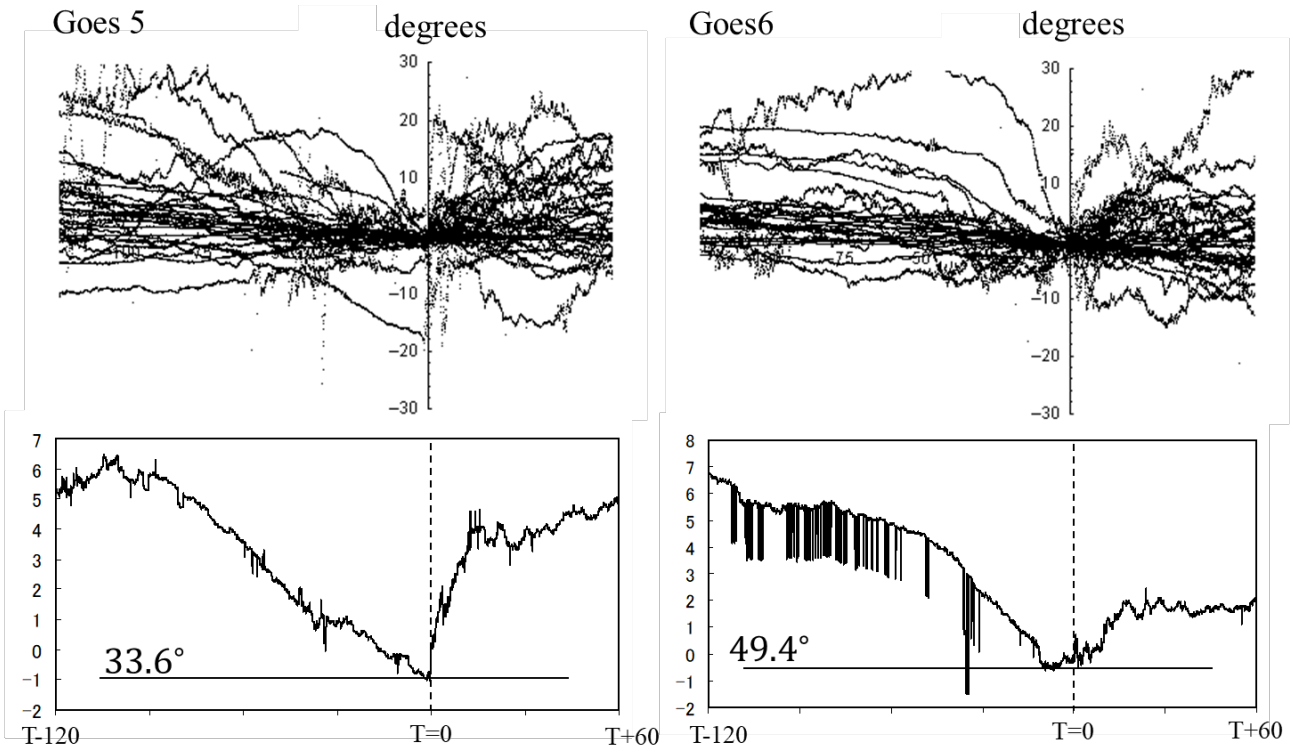
Goes 5
degrees
30
20
10
-10
-20
-30
7
6
5
4
3
2
1
0
-1
-2
33.6°
T-120
T=0
T+60
Goes6
degrees
30
20
10
-10
-20
-30
8
7
6
5
4
3
2
1
0
-1
-2
49.4°
T-120
T=0
T+60

Figure 1

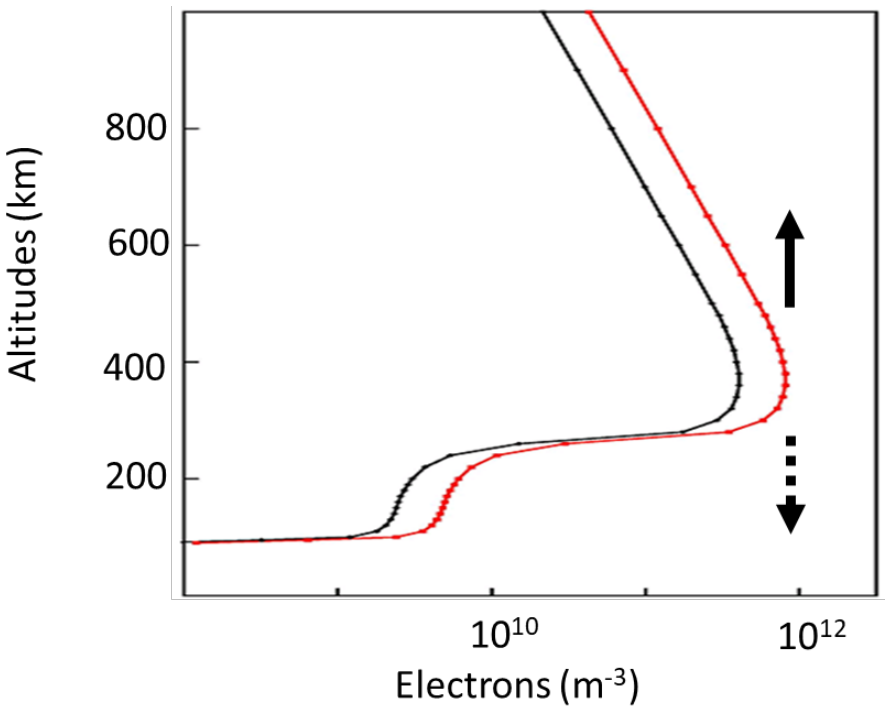

Figure 2

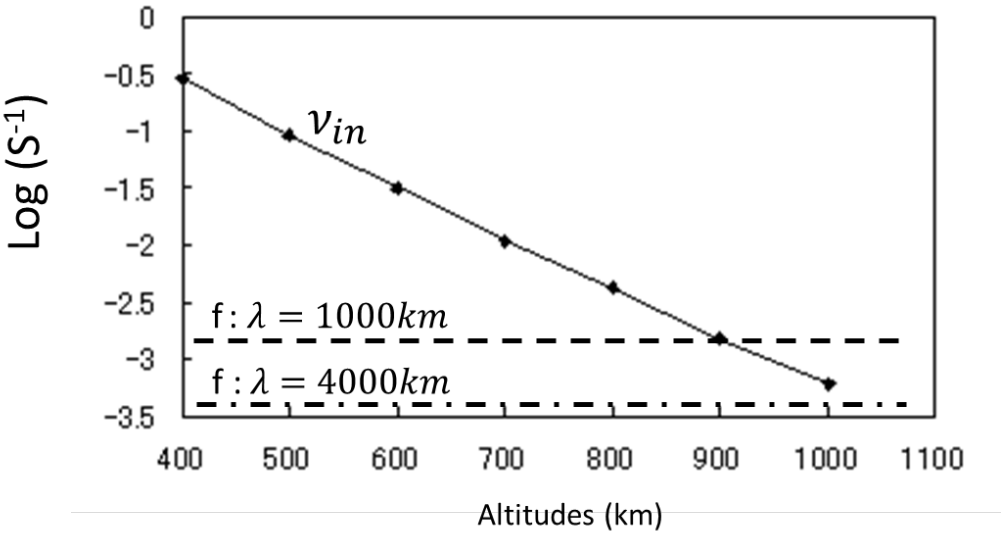
0
-0.5
-1
-1.5
-2
-2.5
-3
-3.5
Log (S^{-1})
ν_{in}
f : $\lambda = 1000km$
f : $\lambda = 4000km$
400
500
600
700
800
900
1000
1100
Altitudes (km)

Figure 3

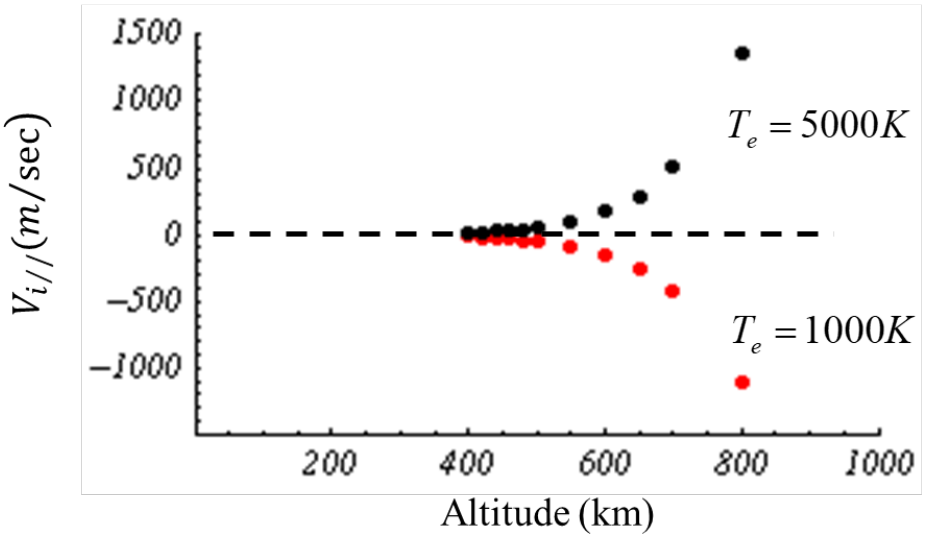
1500
1000
500
0
−500
−1000
200
400
600
800
1000
$V_{i//}(m/\sec)$
$T_e = 5000K$
$T_e = 1000K$
Altitude (km)

Figure 4

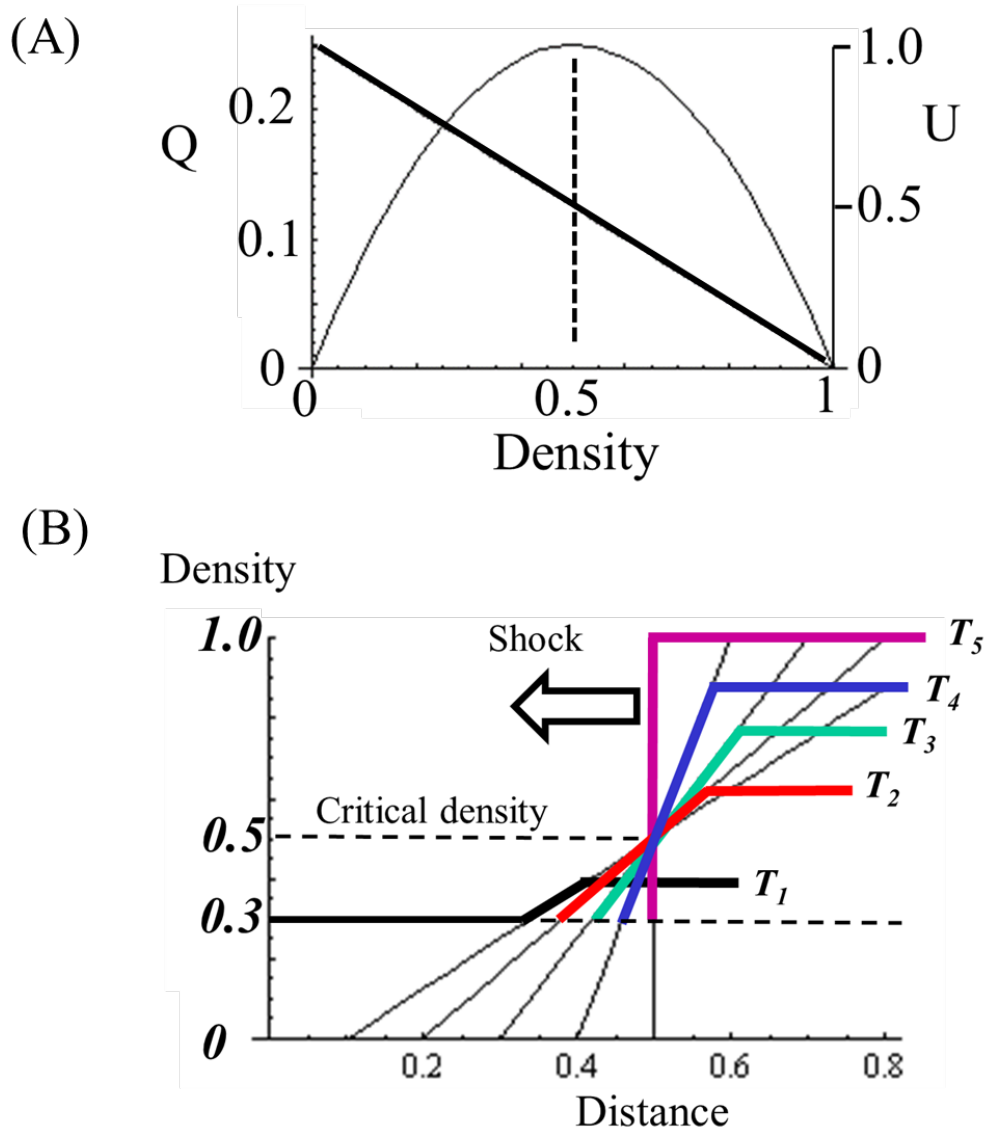
(A)
Q
0.2
0.1
0
0
0.5
1
1.0
U
0.5
0
Density
(B)
Density
1.0
0.5
0.3
0
Shock
Critical density
T_5
T_4
T_3
T_2
T_1
0.2
0.4
0.6
0.8
Distance

Figure 5